Empirical Relationship between Local Scattering Function and Joint Probability Density Function

Michael Walter*, Thomas Zemen♯ and Dmitriy Shutin*
*German Aerospace Center (DLR), Münchener Straße 20, 82234 Weßling, Germany
♯AIT, Austrian Institute of Technology, Donau-City-Straße 1, 1220 Vienna, Austria

***Abstract*—The fading process describing the propagation effects caused by scattering between two mobile transceivers shows strong non-stationary properties. For its characterization the local scattering function (LSF) and the instantaneous delay Doppler probability density function (pdf) have been introduced. In this paper, a relation between LSF and the joint pdf is investigated. In previous works, it was conjectured that a proportionality relationship between LSF and pdf might exist, similar to the relationship between the scattering function and the delay Doppler pdf in the wide-sense stationary uncorrelated scattering case. The goal here is to demonstrate this proportionality empirically based on the analysis of channel measurements. Both the LSF and the delay Doppler pdf can be combined in order to create a model for mobile-to-mobile (M2M) channels. The LSF is hereby used to process the measurement data and extract information like the stationarity time. With this information the joint delay Doppler pdf can be used to create a realistic simulation environment of the wireless channel for M2M communication systems.**

I. Introduction

Mobile-to-mobile (M2M) communications is becoming a very important technology in the twenty-first century. This technology is well exemplified by vehicle-to-vehicle (V2V) communications, where it is one of the key components that enables the implementation of intelligent transportation systems.

In order to develop M2M communications systems, the propagation channel between transmitter (TX) and receiver (RX) needs to be known. There already exists an abundance of models for fixed-to-mobile channels, yet V2V channels are fundamentally different since both TX and RX are mobile and the heights of the antennas on both sides are low. The simultaneous movement of TX and RX makes the M2M channel highly non-stationary, so that the traditional wide-sense stationary uncorrelated scattering (WSSUS) models become inapplicable. Therefore, new channel models have been developed for V2V communications. Most state-of-the-art V2V channel models are geometry-based stochastic models, e.g. [1], where the authors combine some assumptions on the geometry of the considered environment with stochastic methods, such as the placement of the scatterers. The advantage of including assumptions on the geometry is that such channel models are non-stationary, whereas the the stochastic part makes them applicable to different scenarios. In comparison to ray tracing the results might be not as exact for a specific scenario, but more flexible.

The theory of non-WSSUS channels has been addressed in [2]. Matz introduced the LSF in order to describe the time-variant dispersion in delay and Doppler frequency of the channel. Characterization of the V2V channel using the LSF is discussed in [3] and [4]. A conceptually different approach was presented in [5], where the joint delay Doppler pdf is used to characterize V2V channels.

In the classical WSSUS case it is shown [6] that the scattering function, which is a special case of the LSF, is proportional to the joint delay Doppler pdf. In [5] the authors conjectured that a similar proportionality relationship should exist between the LSF and joint delay Doppler pdf in the non-WSSUS case, yet no mathematical proof was provided. Currently it is unknown, whether the proportionality relationship between LSF and delay Doppler pdf exists.

Contributions of this paper: We intend to demonstrate the proportionality of the LSF and the joint delay Doppler pdf empirically by using experimental data collected in a V2V measurement campaign. To this end, we estimate the LSF using collected time-varying channel transfer functions and compare this estimate to the prediction made based on the delay Doppler pdf computation for the same measurement geometry by adapting the delay distribution. The obtained results demonstrate qualitatively a high correspondence of the two models.

The remainder of the paper is structured as follows: In Section II the V2V measurement campaign is described. The calculation of the LSF and its estimation from the measurement data is presented in Section III. The joint delay Doppler pdf and the adaption of the delay pdf to match the LSF is explained in detail in Section IV. The evaluation and comparison of the LSF and joint pdf is performed in Section V. The paper is concluded with Section VI.

II. Measurement Campaign

We conducted a measurement campaign to validate the theoretical model presented in [5]. Furthermore, the measurement data enables us to establish an empirical relationship between the LSF and the joint delay Doppler pdf. The single input single output channel measurements are conducted with two vehicles: a sports utility vehicle that housed the TX, and a van that housed the RX. Both vehicles are shown in Fig. 1.

As measurement equipment a RUSK channel sounder manufactured by MEDAV [7] was used. The key channel sounder parameters are summarized in Table I. The center frequency

TABLE I
Measurement parameters.

Center frequency, f_c	$5.2\,\mathrm{GHz}$
Signal period, τ	$12.8\,\mu\mathrm{s}$
Bandwidth, B	$120\,\mathrm{MHz}$
Delay resolution, $\Delta\tau = 1/B$	$8.33\,\mathrm{ns}$
Measurement time grid, t_s	$1.024\,\mathrm{ms}$
Duration of stationarity region, Mt_s	$123\,\mathrm{ms}$
Max. Doppler frequency, $f_\mathrm{d} = \pm 1/(2t_\mathrm{g})$	$\pm 488\,\mathrm{Hz}$
Doppler resolution, $\Delta f_\mathrm{d} = 1/t_\mathrm{s}$	$8\,\mathrm{Hz}$
Tx/Rx antenna	vehicular dipole antenna
Polarization	vertical
Transmit Power, P_t	$37\,\mathrm{dBm}$ EIRP

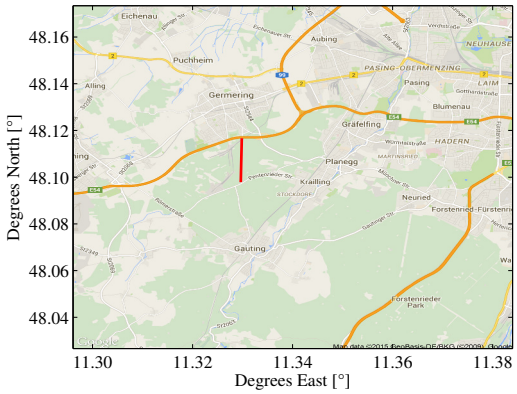

Fig. 1. The measurement route indicated in red on the map. Image by Google, Map Data ©2015 GeoBasis-DE/BKG (©2009).

is at $f_c = 5.2\,\mathrm{GHz}$ with a bandwidth of $B = 120\,\mathrm{MHz}$. The channel is measured every $t_s = 1.024\,\mathrm{ms}$, leading to a maximum Doppler frequency of $f_d = \pm 488\,\mathrm{Hz}$. The latter implies a restriction on the velocity of the transmitter and receiver up to a maximum velocity of $v \leq 14\mathrm{m/s}$ to avoid aliasing. The signals are transmitted with a transmit power of $P_t = 37\,\mathrm{dBm}$ and received via magnetically mounted dipole antennas on the roof of the vehicles. The synchronization of TX and RX is achieved by using a Rubidium atomic clock at each side. A careful calibration of the whole measurement setup is performed before and after each measurement in order to synchronize the clocks and to cancel the influence of the TX and RX hardware components.

In vehicular communications, the environment changes rapidly due to the high mobility of the RX and TX; hence, the channel frequency response $H(t, f)$ is time-varying and frequency-selective, with t and f denoting continuous time and frequency. Due to a multi-carrier (frequency-domain) channel sounding, the equipment outputs a sampled representation of the time-variant channel frequency response:

$$H[m, q] \triangleq H(t_s m, f_s q) \tag{1}$$

where $m \in \{0, \ldots, S-1\}$ and $q \in \{0, \ldots, Q-1\}$ denote the time and frequency indices, respectively. The resolution in the frequency domain is thus given by $f_s = B/Q$ with $Q = 1537$.

The exact positions of TX and RX are recorded using two Septentrio GPS receivers. These highly accurate GPS receivers enable us to extract the geometry of the scatterers in the measured scenario and feed it into the geometric-stochastic channel model (GSCM). The GPS data of the RX is therefore directly stored with the measurement data in the channel sounder. In a post processing step the RX GPS data is related to the corresponding TX GPS data. From a map the width of the scattering zones next to the road can be identified.

The measurements took place on a forested road southwest of Munich, see Fig. 1. Such choice of the measurement location is motivated by the fact that foliage and trees offer an excellent rich scattering environment. Note, that due to limitations on the maximum Doppler frequency, both vehicles had to drive quite slowly, in order not to cause Doppler aliasing. In this paper, we study a single experiment, where both cars drive in opposite

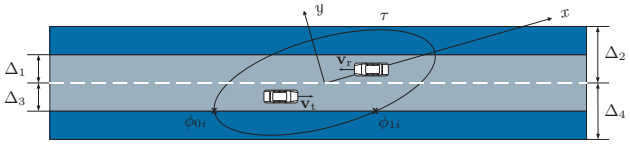

Fig. 2. Geometric set-up of theoretical V2V model.

directions, approaching each other on different lanes with a speed of $\mathbf{v}_t = [32, -0.6]^{\mathrm{T}}\mathrm{km/h}$ and $\mathbf{v}_r = [-31, 0.6]^{\mathrm{T}}\mathrm{km/h}$. The line-of-sight (LOS) distance varies in the interval $d \in [193.22, 195.3]\,\mathrm{m}$. The parameters for the scattering belt are $\Delta_1 = 3.75\,\mathrm{m}$, $\Delta_2 = 11.25\,\mathrm{m}$, $\Delta_2 = 3.75\,\mathrm{m}$ and $\Delta_4 = 11.25\,\mathrm{m}$. Fig. 2 shows the definition of the Δ_i.

III. Local Scattering Function Estimation

In this section, we provide a brief introduction to the background and the calculation of the LSF. A detailed description can be found in [2] and [8].

The observed fading process in vehicular communication channels is non-stationary. Since the environment changes with a finite rate, we can overcome the non-stationarity by approximating the fading process to be locally stationary for a region with finite extent in time and frequency. We assume that the fading process is locally stationary within a stationarity region that has a general extent of $M \times N$ with $M \leq S$ and $N \leq Q$ samples in time and frequency, respectively. Then, we calculate the LSF for consecutive stationarity regions.

The time index of each stationarity region is $k_t \in \{1, \ldots, \lfloor S/M - 1 \rfloor\}$ and it corresponds to the center of the region; similarly, the frequency index is $k_f \in \{1, \ldots, \lfloor Q/N - 1 \rfloor\}$ and it also corresponds to the center of the region. The relative time index within each stationarity region is $m' \in \{-M/2, \ldots, M/2 - 1\}$. The relationship between the relative and absolute time index is given by $m = k_t \cdot M + m'$. Similarly, the relative frequency index within each stationarity region is $q' \in \{-N/2, \ldots, N/2 - 1\}$, and its relationship to the absolute frequency index is given by $q = k_f \cdot N + q'$.

We compute an estimate of the discrete LSF using a multitaper based estimator as follows:

$$\hat{C}[k_t, k_f; n, p] = \frac{1}{IJ} \sum_{w=0}^{IJ-1} \left| \mathcal{H}^{(G_w)}[k_t, k_f; n, p] \right|^2 \tag{2}$$

where $n \in \{0, \ldots, N-1\}$ denotes the delay index, and $p \in \{-M/2, \ldots M/2-1\}$ the Doppler index, respectively. The LSF at (k_t, k_f) corresponds to the center value of the time-frequency stationarity region. The tapered frequency response reads

$$\mathcal{H}^{(G_w)}[k_t, k_f; n, p] = \sum_{m'=-M/2}^{M/2-1} \sum_{q'=-N/2}^{N/2-1} H[m' - k_t, q' - k_f] G_w[m', q'] \mathrm{e}^{-\mathrm{j}2\pi(pm' - nq')}\,. \tag{3}$$

The tapers $G_w[m', q']$ shall be well localized within the support region $[-M/2, M/2-1] \times [-N/2, N/2-1]$. In our application they are computed from I orthogonal time-domain tapers and J orthogonal frequency-domain tapers, resulting in a total of IJ orthogonal two-dimensional tapering functions.

The sequences $u_i[m']$ of the separable taper

$$G_w[m', q'] = u_i[m' + M/2] \tilde{u}_j[q' + N/2] \tag{4}$$

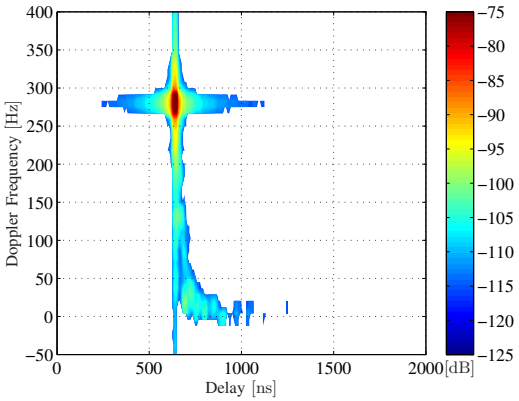

Fig. 3. Estimated LSF $\hat{\mathcal{C}}[k_t, k_f; n, p]$ for two cars driving towards each other on a two lane road. The LOS is indicated by the red color and the contribution by scattering directly follows with decreasing Doppler frequency.

are chosen as the discrete prolate spheroidal sequences (DPSS) [9] with concentration in the interval $\mathcal{I}_M = \{0, \ldots, M-1\}$ and bandlimited to $[-I/M, I/M]$, with $w = iJ + j$, $i \in \{0, \ldots, I-1\}$, and $j \in \{0, \ldots, J-1\}$. The DPSS sequences $u_i[m']$ are defined as the solutions to the Toeplitz matrix eigenvalue equation [9]

$$\sum_{\ell=0}^{M-1} \frac{\sin(2\pi \frac{I}{M}(\ell - m'))}{\pi(\ell - m')} u_i[\ell] = \lambda_i u_i[m'] \,. \tag{5}$$

The sequences $\tilde{u}_j[q']$ are defined similarly, with concentration in the interval $\mathcal{I}_N = \{0, \ldots, N-1\}$ and bandlimited to $[-J/N, J/N]$ such that

$$\sum_{\ell=0}^{N-1} \frac{\sin(2\pi \frac{J}{N}(\ell - q'))}{\pi(\ell - q')} \tilde{u}_j[\ell] = \lambda_j \tilde{u}_j[q'] \,. \tag{6}$$

In contrast to [10] a stationary region with duration $M = 120$ is used (block size), since the evaluation with the LSF showed a smaller duration of the stationarity region [11]. This means that for the calculation of the LSF only $M = 120$ snapshots of the channel are used. Due to the smaller block size the resolution of the Doppler frequency is therefore reduced compared to [10]. The resolution in delay is $\Delta\tau = 1/B = 8.33\,\mathrm{ns}$ and the corresponding Doppler frequency resolution is $\Delta f_\mathrm{d} = 1/(t_\mathrm{s} M) = 8\,\mathrm{Hz}$. The estimated LSF $\hat{\mathcal{C}}[k_t, k_f; n, p]$ for the given scenario is normalized by P_t and shown in Fig. 3, including the LOS. Later, we focus on the scattering.

IV. Joint PDF

The joint pdf of delay and Doppler frequency can be obtained from purely theoretical considerations. In order to incorporate the non-stationarities of the V2V channel, a GSCM is used. The model includes some assumptions on the geometry of the environment, yet considers a random probabilistic relationship between the delay and Doppler frequencies of the scatterers. We briefly revise the most important steps to obtain the joint delay Doppler pdf. A more detailed description can be found in [5].

A. Geometric Part of the Model

The geometric part directly influences the general shape of the delay Doppler pdf, since delay and Doppler are related to the geometry of the scenario. The distance a signal travels from transmitter to receiver via an arbitrary, yet stationary scatterer is given by

$$d(\mathbf{x}, t) = \|\mathbf{x} - \mathbf{x}_\mathrm{t}(t)\| + \|\mathbf{x} - \mathbf{x}_\mathrm{r}(t)\| \,, \tag{7}$$

where $\mathbf{x}$ is the position of the scatterer and $\mathbf{x}_\mathrm{t}(t)$ and $\mathbf{x}_\mathrm{r}(t)$ the time-variant positions of transmitter and receiver, respectively. $\|\cdot\|$ denotes the L^2 norm of a vector. The delay $\tau(\mathbf{x}, t)$ is obtained by dividing the distance $d(\mathbf{x}, t)$ by the speed of light c.

The Doppler frequency f_d is normally calculated using the angle between the direction of movement and the scatterer. Alternatively, it can be expressed as the gradient of the distance multiplied by velocity vectors of TX and RX:

$$f_\mathrm{d}(\mathbf{x}, t) = \left(\mathbf{v}_\mathrm{t}^\mathrm{T} \nabla d_\mathrm{t}(\mathbf{x}, t) + \mathbf{v}_\mathrm{r}^\mathrm{T} \nabla d_\mathrm{r}(\mathbf{x}, t)\right) \frac{f_\mathrm{c}}{c} \,, \tag{8}$$

with $d_\mathrm{t}(\mathbf{x}, t) = \|\mathbf{x} - \mathbf{x}_\mathrm{t}(t)\|$ and $d_\mathrm{r}(\mathbf{x}, t) = \|\mathbf{x} - \mathbf{x}_\mathrm{r}(t)\|$ being the distances of TX to the scatterer and RX to the scatterer, respectively. The representation of the Doppler frequency in Cartesian coordinates allows, after a variable substitution, a delay-dependent description of the Doppler frequency. This relationship is crucial for deriving an instantaneous joint pdf $p(t; \tau, f_\mathrm{d}) = p(\tau) p(f_\mathrm{d}|\tau)$, where the explicit dependency on time in the right-hand side has been dropped for clarity. Now, by considering a specific delay τ, and thus a specific delay ellipse corresponding to τ, we can compute the delay-dependent Doppler frequency by inserting the delay ellipse for an arbitrary but fixed delay into (8). This can be expressed as

$$\begin{aligned} f_\mathrm{d}(\phi|\tau) = {} & \frac{(a_\tau \cos\phi + d/2)}{\sqrt{(a_\tau \cos\phi + d/2)^2 + (b_\tau \sin\phi)^2}} \frac{v_\mathrm{t}^\mathrm{x}}{c} f_\mathrm{c} \\ & + \frac{(a_\tau \cos\phi - d/2)}{\sqrt{(a_\tau \cos\phi - d/2)^2 + (b_\tau \sin\phi)^2}} \frac{v_\mathrm{r}^\mathrm{x}}{c} f_\mathrm{c} \\ & + \frac{b_\tau \sin\phi}{\sqrt{(a_\tau \cos\phi + d/2)^2 + (b_\tau \sin\phi)^2}} \frac{v_\mathrm{t}^\mathrm{y}}{c} f_\mathrm{c} \\ & + \frac{b_\tau \sin\phi}{\sqrt{(a_\tau \cos\phi - d/2)^2 + (b_\tau \sin\phi)^2}} \frac{v_\mathrm{r}^\mathrm{y}}{c} f_\mathrm{c} \,, \end{aligned} \tag{9}$$

with a_τ and b_τ being the semi-major and semi-minor axis of the delay ellipse. The LOS distance between TX and RX is denoted as d. Note, that the ellipse parameter ϕ is *not* identical to the polar angle of the point on the ellipse and the x-axis.

B. Stochastic Part of the Model

After having established a functional relationship between delay and Doppler frequencies, we consider a distribution of f_d and τ by assuming a random distribution of scatterers. The easiest case arises, when the scatterers are assumed to be uniformly distributed. When both TX and RX are moving, the calculation becomes more involved compared to a fixed-to-mobile scenario, since we have to consider the distribution of scatterers located on the selected delay ellipse. This is a two step procedure: first, for a given delay τ, we consider the distribution of the ellipse's parametric angle ϕ, which is given by

$$p(\phi|\tau) = \frac{\sqrt{1 - \epsilon_\tau^2 \cos^2\phi}}{4 \int_0^{\frac{\pi}{2}} \sqrt{1 - \epsilon_\tau^2 \cos^2\zeta} \, \mathrm{d}\zeta} \,, \tag{10}$$

with ϵ_τ being the delay-dependent eccentricity of the ellipse and the denominator an elliptic integral of the second kind. Let us point out that as $\tau \to \infty$, $p(\phi|\tau) \to 1/(2\pi)$, i.e., $p(\phi|\tau)$ converges to a uniform distribution.

In a second step, using (9) we carry out a probability transformation of (10), which makes it possible to determine the delay-dependent Doppler frequency pdf $p(f_\mathrm{d}|\tau)$. The difficulty here is that the relation of ϕ and f_d is a many-to-one mapping. In our case, however, the function can be split into piecewise defined functions. The inverse function is therefore only valid for a certain interval and the Doppler pdf has to be summed over all values of ϕ, which result in the same f_d. The Doppler frequency pdf thus requires evaluating

$$p(f_\mathrm{d}|\tau) = \sum_{\phi' \in \{\mathcal{F}^{-1}(f_\mathrm{d})\}} \frac{p(\phi'|\tau)}{\left|\frac{df_\mathrm{d}}{d\phi'}\right|} \tag{11}$$

with $\mathcal{F}^{-1}(f_\mathrm{d})$ being the piecewise defined inverse function of ϕ and the Doppler frequency f_d. The solutions of ϕ for a given Doppler frequency f_d^* are found numerically by solving an equation $f_\mathrm{d}^* - f(\phi|\tau) = 0$ for ϕ. Note, that there can be a different number of solutions for different f_d^*. With an adequate delay distribution $p(\tau)$, the instantaneous joint pdf $p(t;\tau,f_\mathrm{d}) = p(\tau)p(f_\mathrm{d}|\tau)$ is obtained. In this contribution, we fit $p(\tau)$ to the power delay profile of the scattering process.

Let us again point out that the joint pdf computed in this way is essentially an instantaneous pdf obtained for some arbitrary, yet fixed moment of time t^*. Obviously, as the vehicles are moving, the corresponding pdf $p(t;\tau,f_\mathrm{d})$ will also vary with time, reflecting the non-stationary behavior of the channel.

The last step in calculating the pdf takes into account that only a finite region on the side of the road scatters back the transmitted signal. Therefore, not all of the scatterers on the ellipse can be taken into account, but only a small number of segments. This makes a re-scaling of the pdf necessary. The exact details of the procedure are given in [5]. The re-scaled pdf becomes

$$p(\phi|\tau) = \begin{cases} \frac{\sqrt{1-\epsilon_\tau^2\cos^2\phi}}{\sum_{i=1}^{4}\int_{\phi_{0i}}^{\phi_{1i}}\sqrt{1-\epsilon_\tau^2\cos^2\zeta}\,\mathrm{d}\zeta} & \phi \in \cup_{i=1}^{4}[\phi_{0i},\phi_{1i}] \\ 0 & \text{elsewhere}\,, \end{cases} \tag{12}$$

with ϕ_{0i} and ϕ_{1i} indicating the intersection points of the delay ellipse with the scattering belts on the side of the road, see Fig. 2.

In order to compare the joint delay Doppler pdf and the estimated LSF, we have to consider the time-dependency of the instantaneous pdf. Note, that the computation of the LSF necessarily implies an averaging over a certain window. In contrast, the evaluated pdf gives an instantaneous statistical dependency between delay and Doppler. To be able to compare both methods, we therefore consider a linear combination of the instantaneous delay Doppler pdfs over the same time interval Δt used for computing the LSF.

The resulting temporal mixture is computed as

$$p(\Delta t;\tau,f_\mathrm{d}) = \sum_{i=1}^{P} w_i p(t_i;\tau,f_\mathrm{d})\,, \tag{13}$$

with M being the number of discrete time instances, where the pdfs is evaluated and w_i being the combination weights

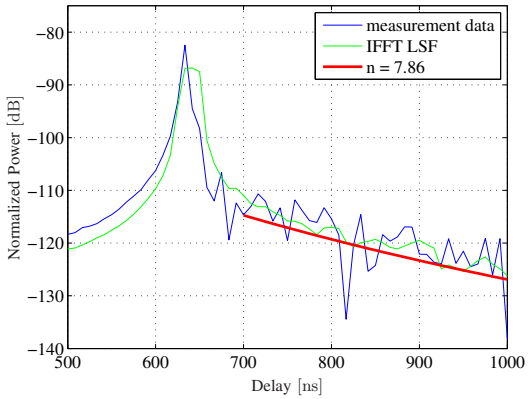

Fig. 4. Estimating the path loss exponent for road side scattering.

chosen so that $\sum_i w_i = 1$. The number M of the pdfs therefore corresponds to the number of snapshots that are used to calculate the LSF. A good agreement between the pdf and LSF was achieved by distributing the weights equally such that $w_i = 1/M, \forall i$. By using a mixture representation, the time-variant behavior of the pdf in this interval is accounted for even though it is the stationarity region of $\Delta t = 123\,\mathrm{ms}$.

V. Comparison

As mentioned already in [5], a comparison between the LSF and the joint pdf is only possible, if an adequate delay distribution is used. Although there are many delay distributions in the literature, most of them cannot be used, since they are only valid for specular propagation paths and not for scattering. For our purposes a dedicated delay distribution for scattering is needed. There are, however, some models dealing with the scattering by foliage and trees, see, e.g., [12].

In this paper, a simple log-distance path loss model is employed similar to the one in [13], proposed for highway, urban, and suburban environments. The path loss exponent $\hat{n}$ is determined empirically by evaluating the impulse response of the V2V channel for the same snapshots as for the LSF. The path loss exponent $\hat{n}$ is evaluated for the scattering that comes after the LOS, i.e., for delays $\tau \in [666, 1000]\mathrm{ns}$. After about $\tau = 1000\,\mathrm{ns}$, the received scattering power is below the noise power and therefore not included in the estimation of $\hat{n}$.

The path loss exponent is calculated by employing a simple least squares algorithm in the double logarithmic domain, where the relation between received power and delay/distance becomes linear.

In Fig. 4, we show both the measurement data and the power delay profile (PDP) calculated with an IFFT of the estimated LSF. Both curves exhibit almost the same slope for the scattering. The broadening of the LOS is due to the finite window length used for estimating the LSF.

The least squares algorithm to determine the path loss exponent $\hat{n}$ is given by

$$\hat{n} = \frac{l\sum_{i=1}^{l} x_i y_i - \sum_{i=1}^{l} x_i \sum_{i=1}^{l} y_i}{l\sum_{i=1}^{l} x_i^2 - \left(\sum_{i=1}^{l} x_i\right)^2}\,, \tag{14}$$

where x_i are the logarithmic values of the squared received amplitude and y_i the logarithmic values of the delay τ. For the

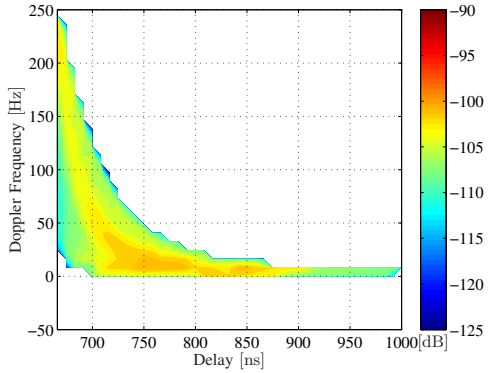

Fig. 5. Zoom of the weighted and scaled joint delay Doppler pdf $p(\Delta t; \tau, f_\mathrm{d})$.

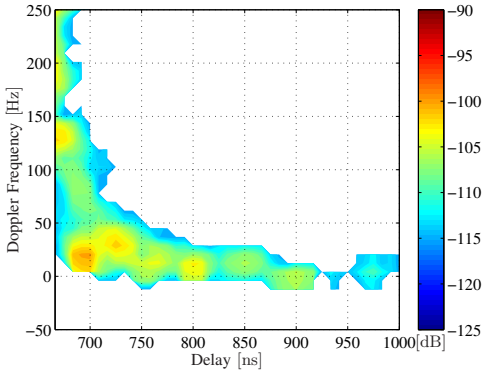

Fig. 6. Zoom of the estimated LSF $\hat{\mathcal{C}}[k_t, k_f; n, p]$ shown in Fig. 3.

given scenario, we obtain a path loss exponent of $\hat{n} = 7.86$, which is in accordance with the values presented in [12]. Note, that the path loss exponent for scattering is much higher than for the LOS, which is approximately the free space path loss exponent of $n_\mathrm{FS} = 2$. The estimated path loss is also displayed in Fig. 4 and it matches both the measurement data and the IFFT of the LSF.

In Figs. 5 and 6 the scaled and weighted joint delay Doppler pdf and the normalized and estimated LSF are compared. We leave out the LOS and consider delays between $\tau \in [666, 1000]\mathrm{ns}$. As mentioned earlier, the scattering power drops below the noise level for $\tau > 1000\,\mathrm{ns}$. The maximum and minimum Doppler frequencies are determined by the geometry of the scenario. A match between LSF and joint pdf is achieved by the correct width of the scattering belts.

The power distribution is determined by the probability distribution of the scatterers. With a uniform distribution of the scatterers on the ellipse, the contributions from the inside of the function, i.e. $\tau \in [700, 850]\mathrm{ns}$ and $f_\mathrm{d} \in [0, 25]\mathrm{Hz}$ is larger than the rest in the joint pdf. The estimated LSF shows a very similar behavior. The LSF, however, is not as smooth as the pdf. One explanation might be a not completely uniform contribution from the foliage or tree trunks resulting in a non-uniform distribution of scatterers in the LSF. The pdf therefore represents a worst case prediction of the scattering, which becomes less severe in the non-uniform case.

The theoretically derived joint pdf can therefore be used to predict the scattering power from the side of the road. Since the scattering effects are highly time-variant, they have a noticeable influence on the performance of a communications system. If the delay distribution $p(\tau)$ is appropriately modeled, the weighted joint pdfs becomes proportional to the estimated LSF $p(\Delta t; \tau, f_\mathrm{d}) \propto \hat{\mathcal{C}}[k_t, k_f; n, p]$, similar to the WSSUS case.

VI. Conclusion

Our empirical analysis shows a qualitative match between the estimated LSF obtained using data from the measurement campaign, and the joint delay Doppler pdf theoretically computed for the same scenario. This generalizes the result from the WSSUS case, where it was shown that the scattering function and the joint delay Doppler pdf are proportional to each other. For simulation purposes this is an important result, since it relates the received scattering power with the corresponding delay Doppler pdf. This relationship allows to use the joint delay Doppler pdf to simulate the V2V channel. Finally, it shows that both the LSF and the joint pdf are related descriptions of non-stationary M2M channels.

References

[1] J. Karedal, F. Tufvesson, N. Czink, A. Paier, C. Dumard, T. Zemen, C. F. Mecklenbräuker, and A. F. Molisch, "A Geometry-Based Stochastic MIMO Model for Vehicle-to-Vehicle Communications," *IEEE Trans. Wireless Commun.*, vol. 8, no. 7, pp. 3646–3657, Jul. 2009.

[2] G. Matz, "On Non-WSSUS Wireless Fading Channels," *IEEE Trans. Wireless Commun.*, vol. 4, no. 5, pp. 2465–2478, Sep. 2005.

[3] A. Paier, T. Zemen, L. Bernadó, G. Matz, J. Karedal, N. Czink, C. Dumard, F. Tufvesson, A. F. Molisch, and C. F. Mecklenbräuker, "Non-WSSUS Vehicular Channel Characterization in Highway and Urban Scenarios at 5.2 GHz Using the Local Scattering Function," in *Int. ITG Workshop on Smart Antennas*, Darmstadt, Germany, Feb. 2008, pp. 9–15.

[4] L. Bernadó, T. Zemen, A. Paier, J. Karedal, and B. H. Fleury, "Parametrization of the Local Scattering Function Estimator for Vehicular-to-Vehicular Channels," in *Proc. IEEE 70th Veh. Technol. Conf.*, Anchorage, AK, USA, Sep. 2009, pp. 1–5.

[5] M. Walter, D. Shutin, and U.-C. Fiebig, "Delay-Dependent Doppler Probability Density Functions for Vehicle-to-Vehicle Scatter Channels," *IEEE Trans. Antennas Propag.*, vol. 62, no. 4, pp. 2238–2249, Apr. 2014.

[6] H. Schulze, "Stochastische Modelle und digitale Simulation von Mobilfunkkanälen," *Kleinheubacher Berichte*, vol. 32, pp. 473–483, 1989.

[7] Medav channel sounder website. [Online]. Available: http://www.channelsounder.de

[8] L. Bernadó, T. Zemen, F. Tufvesson, A. F. Molisch, and C. F. Mecklenbräuker, "Delay and Doppler Spreads of Nonstationary Vehicular Channels for Safety-Relevant Scenarios," *IEEE Trans. Veh. Technol.*, vol. 63, no. 1, pp. 82–93, Jan. 2014.

[9] D. Slepian, "Prolate Spheroidal Wave Functions, Fourier Analysis, and Uncertainty - V: The Discrete Case," *The Bell Syst. Tech. J.*, vol. 57, no. 5, pp. 1371–1430, May-June 1978.

[10] M. Walter, U.-C. Fiebig, and A. Zajic, "Experimental Verification of the Non-Stationary Statistical Model for V2V Scatter Channels," in *Proc. IEEE 80th Veh. Technol. Conf.*, Sep. 2014, pp. 1–5.

[11] L. Bernadó, T. Zemen, F. Tufvesson, A. F. Molisch, and C. F. Mecklenbräuker, "The (in-) validity of the WSSUS Assumption in Vehicular Radio Channels," in *Proc. IEEE 23rd Int. Symp. Personal, Indoor Mobile Radio Commun.*, Sydney, NSW, Australia, Sep. 2012, pp. 1757–1762.

[12] P. Sooksumrarn, C. Kittiyanpunya, P. Yoiyod, and M. Krairiksh, "Wireless Communications in a Tree Canopy," *Progress In Electromagnetics Research B*, vol. 51, pp. 329–346, 2013.

[13] J. Karedal, N. Czink, A. Paier, F. Tufvesson, and A. F. Molisch, "Path Loss Modeling for Vehicle-to-Vehicle Communications," *IEEE Trans. Veh. Technol.*, vol. 60, no. 1, pp. 323–328, Jan 2011.